Diffusivity and Mobility Data

Carelyn E. Campbell, National Institute of Standards and Technology

DIFFUSION is the process by which molecules, atoms, ions, point defects, or other particle types migrate from a region of higher concentration to one of lower concentration. The diffusivity of an atom or diffusion coefficient is the rate at which a particle migrates through a particular material and is dependent on the temperature, composition gradient, and pressure. Diffusivity determines how quickly equilibrium is reached from a nonequilibrium state. In solid-state materials, diffusion can occur by a variety of different mechanisms. Lattice diffusion (bulk or volume diffusion) occurs as a result of individual jumps of atoms or point defects, such as vacancies, divacancies, or interstitials, within the crystal. Diffusion may also occur along the surface or along line defects, such as grain boundaries or dislocations. These line, planar, and surface diffusion mechanisms are generally much faster than the lattice-diffusion-based-mechanisms and, as a result, are termed high-diffusivity paths (or short-circuit diffusivity). Depending on the temperature and/or microstructure of the material, these high-diffusivity paths or bulk diffusion may be the dominate diffusion mechanism. As a wide variety of microstructural processes are controlled by lattice diffusion mechanisms and much of the published diffusion data is for bulk diffusion processes, this article focuses primarily on the diffusivity data and modeling of lattice diffusion in solid-state materials. A list of symbols is in Table 1.

Diffusion Mechanisms

In a crystal, lattice vibrations cause atoms to oscillate around equilibrium positions with frequencies, ν_0 ($\sim 10^{12}$ to 10^{13} Hz); however, occasionally the oscillations are large enough to allow an atom to jump to a different lattice site, resulting in diffusion of the atom. In the absence of a driving force, the energy barrier that an atom must overcome to jump to an empty site is the free energy of migration, G_m. Figure 1 shows the G_m as a function of atomic

Table 1 List of symbols

a	= nearest-neighbor atomic distance (m)
$^k A_i^{pj}$	= contribution to the diffusion-activation energy of component i, in a lattice occupied by p and j atoms in a given phase. k is the order of the interaction parameter (i.e., 0, 1, 2, …) (Eq 27)
b	= thickness of thin layer (Eq 10) (m)
c_i	= volume concentration of component i (mol/m^3)
c_s	= concentration at the surface of semi-infinite solid (Eq 11) (mol/m^3)
c_0	= initial concentration of component at time = 0 s (Eq 10) (mol/m^3)
c_1, c_2	= initial concentrations at the end of infinite couple (Eq 12) (mol/m^3)
c_V^{eq}	= thermal equilibrium vacancy concentration (mol/m^3)
c^-, c^+	= initial compositions of a given diffusion couple (Eq 18) (mol/m^3)
c^*, z^*	= composition at a given distance (z) (Eq 18)
D	= diffusion rate in the absence of any driving force (m^2/s)
D_0	= pre-exponential factor for diffusion (m^2/s)
D_i^*	= tracer diffusion coefficient for component i (m^2/s)
D_i^s	= self-diffusion coefficient for component i (m^2/s)
$^L D_{kj}$	= diffusion coefficient for the diffusing component, j, with respect to the composition gradient of component k, in the lattice-fixed frame of reference (m^2/s)
$^V D_{kj}$	= diffusion coefficient for the diffusing component, j, with respect to the composition gradient of component k, in the volume-fixed frame of reference (m^2/s)
$\tilde{D}_{kj}^n$	= interdiffusion coefficient, where n is the dependent component (m^2/s)
f	= correlation factor for self-diffusion, dependent on crystal structure
g	= geometric factor dependent on the lattice geometry and type of interstitial site
G_m	= free energy of vacancy migration (J/mol)
H_F	= enthalpy of formation of a vacancy (J/mol)
H_m	= enthalpy of vacancy migration (J/mol)
J_i	= flux of particles (number particles per second and unit area) (m^{-2} s^{-1})
$^L J_k$	= flux of particles in the lattice-fixed frame of reference (number particles per second and unit area) (m^{-2} s^{-1})
$^V J_k$	= flux of particles in the volume-fixed frame of reference (number particles per second and unit area) (m^{-2} s^{-1})

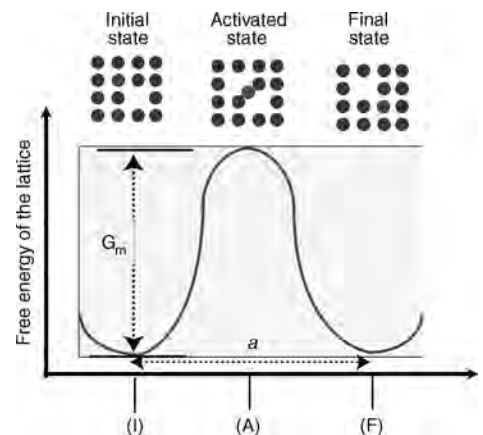|	
M_i	= atomic mobility of component i (m/N/s)
$^L M_{ki}$	= mobility of the diffusing component, k, with respect to the composition gradient of component i, in the lattice-fixed frame of reference
N_i^α	= number of i atoms on the α sublattice
N_{total}^α	= total number of atoms on the α sublattice
p	= probability of the next neighboring site being vacant
ΔQ	= diffusion-activation energy (J/mol)
ΔQ_i^*	= diffusion-activation energy of component i in a given phase (J/mol)
Q_i^j	= diffusion-activation energy of component i in a lattice occupied by pure j atoms in a given phase (J/mol)
$\Delta Q_i'$	= diffusion-activation energy assuming the pre-exponential term is included (J/mol)
ΔQ_k^{ord}	= ordered contribution to the diffusion-activation energy (J/mol)
ΔQ_k^{dis}	= disordered contribution to the diffusion-activation energy (J/mol)
R	= gas constant (J/mol K)
S_F	= entropy of formation of a vacancy (J/K)
S_m	= entropy of vacancy migration (J/K)
t	= time (s)
T	= temperature (K)
V_m	= molar volume of a phase (m^3/mol)
x_i	= mole fraction of component i
y_i^α, y_i^β	= site fractions of component i on the α and β sublattices, respectively
Y_i	= normalized concentration variable (Eq 16)
z	= distance (m)
z_K	= position of the Kirkendall plane (m)
z_M	= position of the Matano plane (m)
δ_{ik}	= Kronecker delta symbol, equals 1 when $i = k$ and 0 when $i \neq k$
Φ_i	= pre-exponential factor defining the mobility of atom i
Γ	= jump frequency (s^{-1})
λ	= diffusion length (m)
μ_i	= chemical potential of component i (J/mol)
ν_0	= equilibrium lattice frequency (Hz) (s^{-1})
π	= constant, 3.14…
υ_K	= Kirkendall velocity (m/s)
ω	= jump rate for atom to a neighboring empty lattice site

Fig. 1 Assuming no driving force on an atom, a schematic of the energy barrier that must be overcome for a diffusion to occur. I, initial state; A, activated state, F, final state

position. The jump rate, ω, for an atom to jump to a neighboring empty site is given by:

$$\omega = \nu_0 \exp\left(-\Delta G_m / RT\right) \text{where } \Delta G_m = H_m - TS_m$$

(Eq 1)

where ν_0 is the atomic vibration frequency, R is the gas constant, T is the temperature in Kelvin, and H_m and S_m are the enthalpy and entropy of migration. The jump frequency, Γ, of an atom is then defined as the jump rate times the probability, p, of the next neighboring site being vacant:

$$\Gamma = \omega p$$

(Eq 2)

Two of the most common mechanisms by which atoms diffuse are interstitial diffusion and vacancy diffusion. Interstitial diffusion occurs as small interstitial atoms, which are solute atoms that are considerably smaller than the solvent atoms, jump from one interstitial site to the next-nearest unoccupied interstitial site. Thus, for a dilute interstitial alloy, the probability defined in Eq 2 is approximately equal to 1, and the diffusion rate in the absence of any driving force (concentration gradient) is:

$$D = \left[ga^2\nu_0 \exp\left(\frac{S_m}{R}\right)\exp\left(\frac{-H_m}{RT}\right)\right]$$

(Eq 3)

where a is the nearest-neighbor atomic distance, and g is a geometric factor that depends on the lattice geometry and the type of interstitial site (i.e., octahedral or tetrahedral). This expression is commonly simplified to an Arrhenius-type equation:

$$D = D_0 \exp\left(\frac{-\Delta Q}{RT}\right) \text{ where } D_0$$
$$= ga^2\nu_0 \exp\left(\frac{S_m}{R}\right) \text{ and } H_m = \Delta Q$$

(Eq 4)

Vacancy-driven diffusion occurs when a nearest-neighbor atom (substitutional solute atom) jumps onto an unoccupied lattice site. The probability of the nearest-neighbor site being vacant, p from Eq 2, is defined by the thermal equilibrium vacancy concentration, c_V^{eq}, which is given by:

$$c_V^{eq} = \exp\left(\frac{S_F}{R}\right)\exp\left(\frac{-H_F}{RT}\right)$$

(Eq 5)

where S_F and H_F are the formation entropy and enthalpy, respectively, of a vacancy. Thus, similar to Eq 3 for the interstitial diffusion rate, the substitutional diffusion rate in the absence of a driving force is given by:

$$D = \left[fa^2\nu_0 \exp\left(\frac{S_F + S_m}{R}\right)\exp\left(\frac{-(H_F + H_m)}{RT}\right)\right]$$

(Eq 6)

where f is the correlation factor that determined by the crystal structure. Like Eq 3, 6 can be written in terms of an Arrhenius relation, where:

$$D_0 = fa^2\nu_0 \exp\left(\frac{S_F + S_m}{R}\right)$$

and $\Delta Q = H_F + H_m$. It should be noted that while these Arrhenius-type relations (Eq 4 and 6) are common, they are not universal. Grain-boundary, impurities, or other microstructural features; temperature-dependent activation parameters; and other active diffusion mechanisms may all result in deviations from an Arrhenius relation.

Diffusion Equation

In a steady-state one-dimensional system, the flux of particles is proportional to the concentration gradient:

$$J_i = -D_i \frac{\partial c_i}{\partial z}$$

(Eq 7)

where J_i describes the amount of material that passes through a unit area of a plane per unit time (t) within a volume-fixed frame of reference (otherwise known as flux). The variable D_i is the diffusivity of component i for a given diffusion mechanism. The variable c_i is the concentration of particles i (Note: $c_i = x_i V_m$, where x_i is the mole fraction of component i, and V_m is the molar volume of the phase), and z is the diffusion distance. Equation 7, better known as Fick's law (Ref 1, 2), assumes there are no external forces or driving forces acting on the particles and is formally identical to Fourier's law of heat conduction and Ohm's law of current flow.

For a nonsteady-state one-dimensional system where the flux at each point varies with time, Fick's law must be combined with a mass balance or continuity equation (Eq 8) to determine the time-dependent concentration, where t is the time in seconds:

$$\frac{\partial J}{\partial z} = -\frac{\partial c}{\partial t}$$

(Eq 8)

Equations 7 and 8 are combined to form the general diffusion equation, which is a second-order linear partial differential equation and cannot be solved analytically:

$$\frac{\partial c_i}{\partial t} = \frac{\partial}{\partial z}\left(D_i \frac{\partial c_i}{\partial z}\right)$$

(Eq 9)

However, if D_i is assumed to be concentration independent, the diffusion equation can be solved for a variety of initial and boundary conditions, as demonstrated by Ref 3 and 4. Two simple examples of these solutions that are commonly used experimentally are the thin-film and error-function solutions.

The thin-film solution assumes that a thin layer, with a thickness, b, of the diffusing species A is concentrated at $z = 0$ of a semi-infinite sample, as seen in Fig. 2. Then, concentration profiles after time, t, are given by:

$$c(z,t) = \frac{bc_0}{\sqrt{\pi Dt}}\exp\left(-\frac{z^2}{4Dt}\right)$$

(Eq 10)

where c_0 is the initial concentration of the A layer. The diffusion length, λ, is represented by the $\sqrt{Dt}$ quantity and is a characteristic length used in solving diffusion equations. The thin-film solution is valid for applications where λ is much greater than the initial layer thickness. The geometry represented by the thin-film solution (Eq 10) is commonly used to measure tracer diffusion coefficients in substitutional alloys (defined in the section "Tracer Diffusivity" in this article).

Infinite and Semi-Infinite Solutions. Error-function solutions can be applied to semi-infinite and infinite samples. The concentration profiles in a semi-infinite solid with a constant concentration of a component at the surface, c_s, are defined by the following error functions and initial and boundary conditions:

Initial conditions: $t = 0$; $z > 0$; $c(z,0) = c_0$, where c_0 is the initial concentration in the solid

Boundary conditions: at all $t > 0$, z = 0; $c(0,t) = c_s$

The concentration profile for a given time is then given by:

$$\frac{c - c_s}{c_0 - c_s} = \mathrm{erf}\left(\frac{z}{2\sqrt{Dt}}\right)$$

(Eq 11)

These types of solutions are applicable to modeling various carburization and coating problems.

For an infinite sample with a concentration profile defined by a step function, the composition profile at given time, t, is:

$$\frac{c - c_1}{c_2 - c_1} = \frac{1}{2}\mathrm{erfc}\left[\frac{z}{2\sqrt{Dt}}\right]$$

(Eq 12)

where the initial boundaries at $t = 0$ are given by:

$$t = 0 \begin{cases} z\langle 0 & c = c_2 \\ z\rangle 0 & c = c_1 \end{cases}$$

and c_1 and c_2 are the compositions at either end of the infinite couple, as seen in Fig. 3. This type of solution is often used when the diffusion distances in the two materials are much smaller than the width of the samples. While analytical solutions to the diffusion equation assuming a constant diffusivity are useful in solving some practical problems, to solve most problems of interest, the composition and temperature dependence of the diffusivity must be considered, and the equation must be solved numerically.

Diffusion Data

Diffusivity in a material can be evaluated in variety of different ways, including measurement of diffusion coefficients, composition profiles, and layer growth widths. Tracer, intrinsic, and chemical diffusivities can all be extracted from various types of direct and indirect diffusion experiments. Table 2 reviews some of the common direct and indirect methods to measure these diffusion coefficients. Direct experiments are based on Fick's law (Eq 7) and the phenomenological definitions of the diffusion coefficients. Indirect experimental methods are not based on Fick's law and require a microscopic model of the atomic jump processes to deduce a diffusion coefficient.

Tracer Diffusivity. Tracer diffusion is the migration of a tagged atom through a material

of which it is a component. As such, the tracer diffusivity is generally measured by introducing a radioactive isotope in dilute concentration into an otherwise homogeneous material. Thus, the only driving force in the system is that of the concentration gradient of the tracer. In a homogenous material, the mean square displacement of the tracer in the z-direction is defined by the Einstein formula for Brownian motion (random walk) as:

$$\langle z_i^2 \rangle = 2D_i^* t \text{ where } D_i^* = RTM_i \qquad \text{(Eq 13)}$$

where D_i^* is the tracer diffusion coefficient, t is the diffusion time, and M_i is the atomic mobility of the i atoms or the movement of atoms in response to a given force, in this case, the result of continuous random movement. (Note that for a multicomponent alloy, the mobility

is a function of each component in the alloy. Further description of the calculation of the composition-dependent mobility matrix is given in the section "Disordered Phase" in this article.) The tracer diffusion coefficient is equal to the self-diffusion coefficient, D_i^S, if diffusion takes place by uncorrelated atomic jumps; otherwise, the tracer diffusion coefficient is related to the self-diffusion coefficient by the correlation factor, f, $D_i^* = fD_i^S$. The correlation factor is dependent on crystal structure and introduces off-diagonal terms into the M_i matrix. For the body-centered cubic (bcc) and face-centered cubic (fcc) crystal structures assuming a vacancy-diffusion mechanism, the contribution of these off-diagonal terms is small. Thus, for simplicity, these terms are not included in the present discussion; however, calculation methods are discussed by Ref 5 and 6. When a tracer impurity is measured in a homogeneous material (i.e., solute C in a pure A alloy or homogeneous AB alloy), the measured tracer diffusivity is often referred to as the impurity diffusivity.

Chemical Diffusivity (Interdiffusion). In contrast to tracer diffusivity measurements that only consider negligible amounts of a tracer element in an otherwise homogeneous material, interdiffusion (chemical diffusion) and intrinsic diffusion coefficient measurements are performed in nonhomogeneous materials where the diffusion flux is proportional to the gradient of the chemical potential (e.g., in the presence of a driving force). The interdiffusion coefficient, $^V D_{kj}$, is defined in the volume-fixed frame of reference, where the sum of the fluxes equals zero, and is given by:
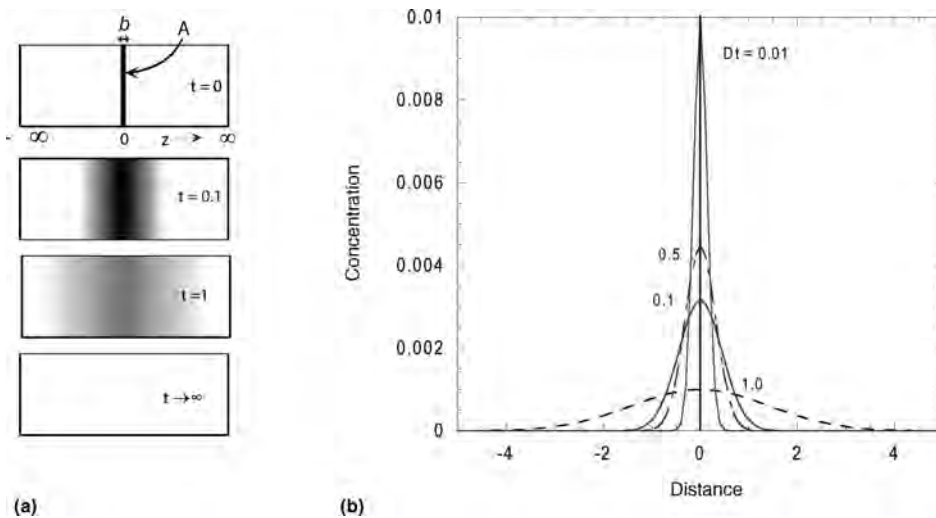

Fig. 2 Schematic of (a) thin-film geometry and (b) solution. (a) A thin layer of the diffusing species (*A* atoms per unit area) is concentrated at *z* = 0. As time increases, the *A* atoms diffuse such that concentration becomes negligible. (b) The concentration of *A* atoms as a function of distance for different times, where the time increments are given as *D**t, where *D* is a constant.

Table 2 Direct and indirect methods for measuring diffusion coefficients

| Method	Δx	D, m^2/s
Direct		
Lathe sectioning, grinding	0.1–250 μm	10^{-19} to 10^{-10}
Microtome	1–10 μm	10^{-17} to 10^{-12}
Chemical	10 μm	10^{-15} to 10^{-12}
Electrochemical	50 nm	10^{-20} to 10^{-17}
Sputtering	5–100 nm	10^{-22} to 10^{-17}
Modulated structures	0.5–5 nm	$\geq 10^{-26}$
Ion microprobe (secondary ion mass spectroscopy)	1–100 nm	10^{-23} to 10^{-17}
Electron microprobe	≥ 2 μm	10^{-16} to 10^{-12}
Rutherford backscattering	50 nm	10^{-20} to 10^{-17}
Nuclear reaction analysis	20–100 nm	5×10^{-21} to 5×10^{-16}
Indirect		
Nuclear magnetic resonance	...	10^{-20} to 10^{-9}
Neutron inelastic scattering	...	10^{-11} to 10^{-9}
Mossbauer effect	...	10^{-15} to 10^{-11}
Conductivity (ionic crystals)	...	10^{-17} to 10^{-10}
Resistivity (semiconductors)	...	10^{-20} to 10^{-12}
Elastic after-effect	...	10^{-25} to 10^{-21}
Internal friction	...	10^{-20} to 10^{-15}
Magnetic anisotropy	...	10^{-25} to 10^{-21}

Source: Ref 5
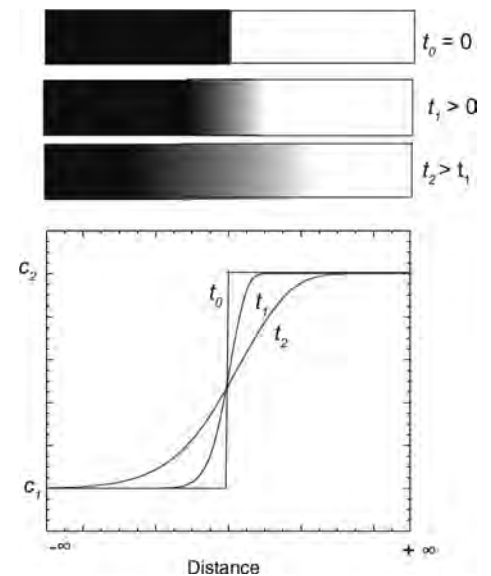
Fig. 3 Example of error-function solutions for an infinite couple with initial end-member compositions of c_1 and c_2. The composition profiles show the diffusion of the species with increasing time.

$$\sum_{k=1}^{n} {}^{\mathrm{V}}J_k = 0 \qquad\qquad \text{(Eq 14)}$$

$${}^{\mathrm{V}}D_{kj} = \sum_{i=1}^{n} (\delta_{ik} - x_k) x_i M_i \frac{\partial \mu_i}{\partial x_j} V_{\mathrm{m}} \qquad \text{(Eq 15)}$$

The component j is the diffusing component, and k is the gradient component. The δ_{ik} is the Kronecker delta symbol and equals 1 when $i = k$ and 0 when $i \neq k$. The partial derivative of the chemical potential, μ_i, with respect to the mole fraction, x_i, corresponds to the thermodynamic factor. Note that the partial derivative of the chemical potential can be easily calculated using a functional representation of the Gibbs energy, for example, an appropriate multicomponent thermodynamic database. However, the thermodynamic factor must be evaluated in the form $\mu_k(x_1, x_2, \ldots x_n)$ because there are n-1 independent concentrations. As there are only (n-1) independent components, diffusion couple experiments are only able to directly evaluate the interdiffusion coefficient, $\tilde{D}_{kj}^{n}$:

$$\tilde{D}_{kj}^{n} = D_{kj}^{\mathrm{V}} - D_{kn}^{\mathrm{V}} \qquad\qquad \text{(Eq 16)}$$

where n is the dependent variable. Using these interdiffusion coefficients, the flux equations (Eq 7) in the volume-fixed frame of reference, where the sum of the fluxes equals zero, can be written as:

$$J_k = -\sum_{j=1}^{n-1} \tilde{D}_{kj}^{n} \frac{\partial c_j}{\partial z} \qquad\qquad \text{(Eq 17)}$$

There are several methods for determining interdiffusion coefficients from measured composition profiles from diffusion couple experiments. Figure 4 shows that for diffusion couples that can be approximated as an infinite medium, the Boltzmann-Matano method (Ref 7, 8) can be used to determine the interdiffusion coefficients from experimental composition profiles at a given time, t:

$$\tilde{D}(c^*) = \left(2t \frac{dc}{dz}\bigg|_{z^*} \right)^{-1} \int_{c}^{c^*} (z_M - z)\, dc \text{ and}$$

$$\int_{c^-}^{c^+} (z_M - z)\, dc = 0 \qquad\qquad \text{(Eq 18)}$$

The variable z_{M} defines the Matano plane through which equal amounts of material have moved in the positive and negative directions. The concentrations c^- and c^+ represent the initial compositions of the diffusion couple. However, this commonly used method does not consider the change in molar volume across the diffusion couple. When significant molar volume changes are present (e.g., in the intermetallic NiAl-B2, Ref 9), the interdiffusion coefficients should be calculated using methods that include the composition dependence of the molar volume, such as that proposed by Ref 10 to 12:
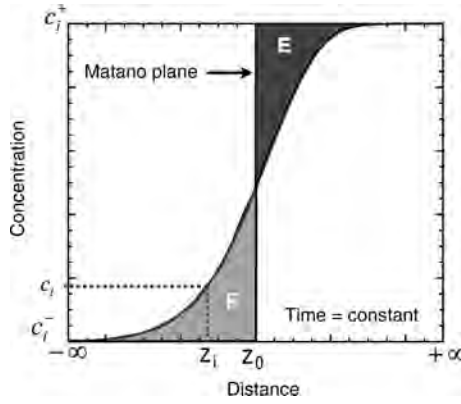
Fig. 4 Example of Boltzmann-Matano calculation for a single-phase interdiffusion experiment with end-member composition of c_i^- and c_i^+. The Matano plane is located at z_0 and is chosen such that the two shaded areas, E and F, are equal. The diffusion coefficient at given c_i concentration is then given by Eq 18.

$$\tilde{D} = \frac{V_{\mathrm{M}}}{2t} \left(\frac{dz}{dY_i} \right)_{Y^*} \left[(1 - Y_i^*) \int_{-\infty}^{z^*} \frac{Y_i}{V_{\mathrm{M}}} dz \right.$$

$$\left. + Y_i^* \int_{z*}^{-\infty} \frac{(1 - Y_i)}{V_{\mathrm{M}}} dz \right] \text{ where } Y_i = \frac{(c_i - c_i^-)}{(c_i^+ - c_i^-)}$$

$$\text{(Eq 19)}$$

where Y_i is a normalized concentration variable. This method also eliminates the need to determine a Matano interface, which is often a source of error. An example of the method is shown in Fig. 5 for a cobalt-nickel diffusion couple.

As the number of elements in the diffusion couples increases, determining the interdiffusion coefficients becomes more difficult; for each interdiffusion coefficient, ($n-1$) composition profiles with different terminal compositions must intersect at one common intersection point. In an effort to overcome this complexity, Ref 13 derived a new analysis method that enables the determination of an average interdiffusion coefficient over a selected composition range from a single multicomponent diffusion couple by integrating the interdiffusion flux of a component over the diffusion distance for a selected range of compositions. This method has been implemented in the computational software program MultiDiFlux (Ref 14). (Commercial products are referenced in this paper as examples. Such identification does not imply recommendation or endorsement by the National Institute of Standards and Technology.)

Intrinsic Diffusivity. The intrinsic diffusion coefficient defines the diffusion of a component relative to the lattice planes and is the product of the diffusion mobility and the thermodynamic factor in the lattice-fixed frame of reference, where the sum of the diffusion fluxes equals the vacancy flux:

$$\sum_{k=1}^{n} {}^{\mathrm{L}}J_k = -{}^{\mathrm{L}}J_{\mathrm{vacancy}} \qquad\qquad \text{(Eq 20)}$$
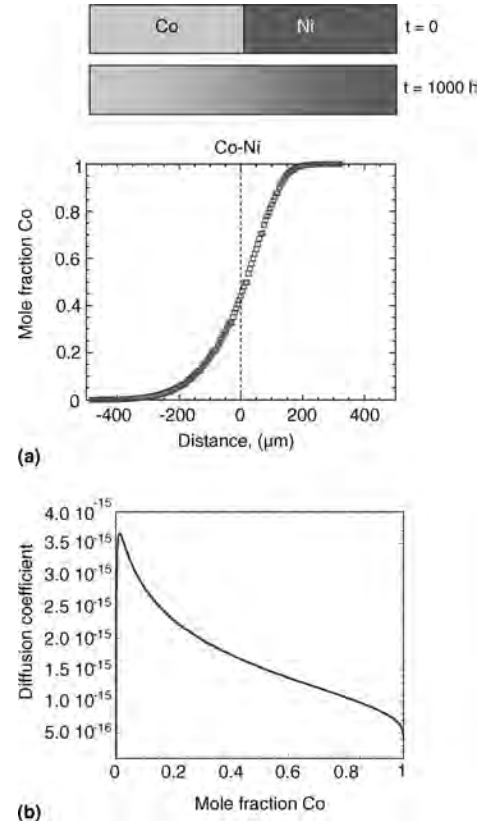
Fig. 5 Example of the Sauer-Freise method to calculate the interdiffusion coefficient for face-centered cubic cobalt-nickel at 1150 °C. (a) Measured composition profile after 1000 h at 1150 °C. (b) Calculated interdiffusion coefficient at 1150 °C. Source: Ref 10

$${}^{\mathrm{L}}D_{kj} = \sum_{i=1}^{n} \delta_{xi} x_i M_k \frac{\partial \mu_k}{\partial x_j} \qquad\qquad \text{(Eq 21)}$$

A net flux of atoms across any lattice plane occurs during interdiffusion as the diffusion rates of the components in a material are different. Thus, there is a shift of lattice planes relative to a fixed lattice axis, which is known as the Kirkendall effect. This shift of lattice planes is observed by placing inert markers at the initial interface of a diffusion couple (Fig. 6) (Ref 15, 16). The velocity of the inert markers equals the Kirkendall velocity. Thus, the difference between Eq 15, ${}^{\mathrm{V}}D_{kj}$, and Eq 21, ${}^{\mathrm{L}}D_{kj}$, is the reference state. The ${}^{\mathrm{V}}D_{kj}$ represents the measurement of the diffusivity relative to a fixed position, while the ${}^{\mathrm{L}}D_{kj}$ represents the measurement of diffusivity relative to a fixed lattice plane. This difference in the frame of reference is similar to measuring the speed of a train when the observer is standing at a fixed position on the train platform (in the volume-fixed frame of reference) versus when the observer is sitting in one of the train cars (the lattice-fixed frame of reference).

For a substitutional binary alloy, the intrinsic and tracer diffusivities are related to the interdiffusion coefficient and the Kirkendall

velocity. For example, for a binary AB alloy, Darken (Ref 17) deduced the following approximate relations, which disregard the coupling between the fluxes of the two atoms and the vacancy flux:

$$^{V}\tilde{D}_{AB} = x_B\,^{L}D_A + x_A\,^{L}D_B = \left(x_A D_B^* + x_B D_A^*\right)\frac{\partial\mu_A}{\partial x_B}$$
(Eq 22)

The Kirkendall velocity, v_K, is given by:

$$v_K = \left(^{L}D_A - ^{L}D_B\right)\frac{\partial x_A}{\partial z}$$
(Eq 23)

For a more complete description of the relationship between the diffusivities in a "random" alloy during a vacancy-driven diffusion process, the Darken-Manning relations (Ref 18, 19) should be used.

As an example of the relationship between the diffusivities, consider the fcc diffusivities for the iron-nickel system at 1200 °C (Fig. 7). Figure 7 (a) shows the calculated thermodynamic factors, and Fig. 7(b) shows the mobilities for nickel and iron. The Darken relationship (Eq 22) is demonstrated in Fig. 7(c):

$$\tilde{D}_{FeNi} = x_{Fe}\,^{L}D_{Ni} + x_{Ni}\,^{L}D_{Fe}$$
(Eq 24)

where the intrinsic lattice diffusivities, Eq 21, $\left(^{L}D_{Ni}, ^{L}D_{Fe}\right)$ are calculated by multiplying the thermodynamic factor (Fig. 7a) by the mobility (Fig. 7b).

First-Principles Data. In addition to the variety of experimental methods available for measuring diffusivity, first-principles calculations may be available to help estimate difficult-to-measure or metastable diffusion coefficients. Density-functional methods can be used to calculate the self-activation diffusion energies (Ref 20). Embedded-atom potentials can be used to evaluate diffusion mechanisms and determine activation energies (Ref 21–23). Diffusion coefficients can be extracted from kinetic Monte Carlo simulations using Kub-Green expressions (Ref 24, 25).

Modeling Multicomponent Diffusivity Data

While much of the diffusivity data for the pure elements and many binary alloys have been measured and are available in the literature, diffusivity data for multicomponent systems are scarce and difficult to measure. Experimentally determining all the needed diffusion coefficient matrices for a multicomponent diffusion simulation is simply not practical or efficient. However, these multicomponent data are critical for correctly predicting diffusion behavior in many industrial (commercial) applications and may be strongly dependent on composition. Thus, multicomponent diffusion mobility databases are developed to predict the needed bulk diffusion coefficients.
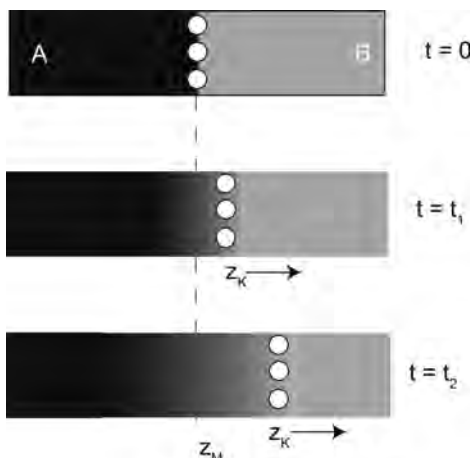

Fig. 6 Schematic of Kirkendall effect in an A-B diffusion couple where the B atoms diffuse faster than the A atoms ($D_B > D_A$), and the interface moves to the right. The Matano plane is defined by z_M, and the Kirkendall plane is located at z_K.

Using Onsager's relations and a Calphad-based method (Ref 26–28), Ref 29 developed a formalism to describe diffusion mobilities in multicomponent systems and to develop multicomponent diffusion mobility databases. These diffusion mobilities can then be combined with the needed thermodynamic factors to calculate the multicomponent diffusion coefficients. Appendix 1 demonstrates how ternary tracer, intrinsic, interdiffusion coefficients are calculated for a given set of diffusion mobilities and chemical potentials.

Disordered Phase

Substitutional Diffusion. Assuming a vacancy diffusion mechanism in a crystalline phase, the mobility matrix in the lattice-fixed frame, $^{L}M_{ki}$, which is both composition and temperature dependent, can be written in terms of an Arrhenius-type relation similar to Eq 4 and 6:

$$^{L}M_{ki} = \delta_{ki}x_i M_i$$
(Eq 25)

$$M_i = \Theta_i \frac{1}{RT}\exp\left(\frac{\Delta Q_i^*}{RT}\right)$$
(Eq 26)

Following the work of Ref 29, the off-diagonal terms of the diffusion mobility matrix are assumed to be zero; that is, correlation effects are assumed to be negligible. M_i is the mobility of component i in a given phase (this is the same M_i as in Eq 13, 15, and 21), Θ_i represents the effects of the atomic jump distance (squared) and the jump frequency, and ΔQ_i^* (with units of J/mol) is the diffusion-activation energy of component i in a given phase. The partial molar volumes are assumed to be constant, and the composition and temperature dependence of each ΔQ_i^* are expressed in terms of a Redlich-Kister (Ref 30) polynomial (Ref 29, 31–35):
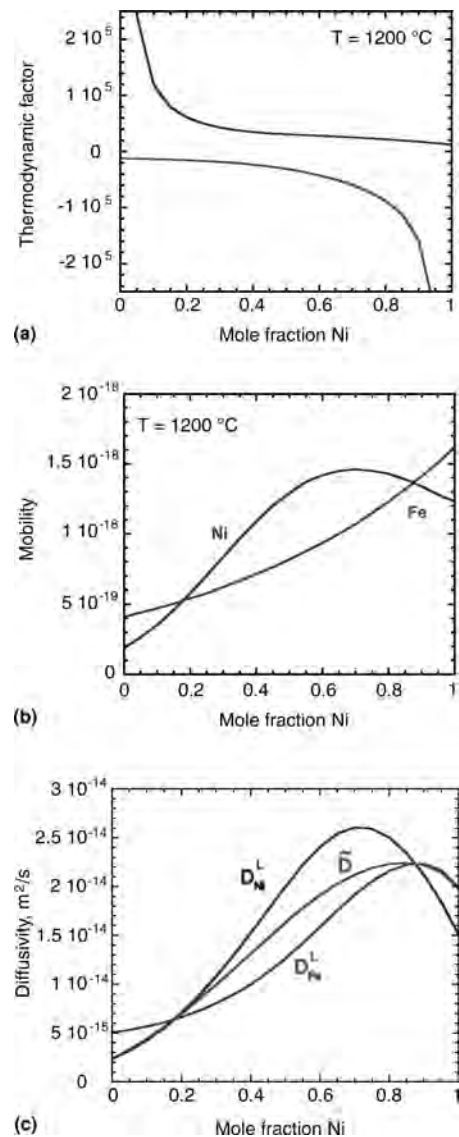

Fig. 7 Example of the calculation of the intrinsic diffusion and interdiffusion coefficients for the iron-nickel system at 1200 °C. Thermodynamic factors (a) and mobilities (b) for iron and nickel as functions of composition are multiplied to calculate the intrinsic diffusion coefficients shown in (c). The Darken relation (Eq 22) is used in (c) to calculate the interdiffusion coefficient.

$$\Delta Q_i^* = \sum_j x_j Q_i^j + \sum_p \sum_{j>p} x_p x_j \sum_k {}^{k}A_i^{pj}\left(x_p - x_j\right)^k$$
(Eq 27)

where Q_i^j and $^{k}A_i^{pj}$ are linear functions of temperature. The expansion of the composition dependence in terms of a Redlich-Kister polynomial is similar to the development of thermodynamic databases with the Calphad method (Ref 26–28). Note that for a given diffusing component, i, if all Q_i^j are equal and $^{k}A_i^{pj}$ equals zero, then ΔQ_i^* and the corresponding M_i are not concentration dependent. The composition dependence of Θ_i can also be

represented by Eq 27. If there is no ferromagnetic contribution, it is frequently assumed that Θ_i depends exponentially on composition (Ref 36), and it is included in the activation energy term. With this assumption, Eq 26 can be written as:

$$M_i = \frac{1}{RT}\exp\left(\frac{\Delta Q_i'}{RT}\right)$$

where $\Delta Q_i' = \Delta Q_i^* - RT\ln\Theta_i$ (Eq 28)

Interstitial Diffusion. Interstitial elements can be added to the database by using a sublattice description and by assuming the partial molar volume of the interstitial element is zero (Ref 37). An example of this model is the addition of carbon to the Fe-Ni-Cr fcc phase in the diffusion assessment by Ref 38.

Magnetic Transition. For substitutional elements in bcc alloys, such as transition metals, the effect of the transition between the para- and ferromagnetic states contributes to the diffusion. The effect of magnetic ordering on diffusion can be included (Ref 39, 40), using the model of Braun and Feller-Kniepmeier (Ref 41), which relates the change in diffusivity to the magnetic enthalpy. For interstitial elements, such as carbon or nitrogen, the effect of the magnetic transition is less well established. The magnetic transition has a strong effect on carbon diffusivity (Ref 42), which can be modeled by applying the same activation energy to both the paramagnetic and ferromagnetic states (Ref 43). However, no significant change in the nitrogen diffusivity is observed as the magnetic transition occurs.

Ordered Phases

For an ordered phase, the composition dependence of the diffusion mobilities must include the effect of chemical ordering. Based on the model by Girifalco (Ref 44), which assumes the activation energy from chemical ordering is dependent on a long-range order parameter, the effect of chemical ordering is included by dividing the activation energy into two terms (Ref 35). The first term represents the contribution from the disordered state, ΔQ_k^{dis}, and the other term represents the contribution from the ordered state, ΔQ_k^{ord}, which is based on a long-range order-type parameter, the site fraction of a given component i:

$$\Delta Q_k = \Delta Q_k^{\text{dis}} + \Delta Q_k^{\text{ord}}$$ (Eq 29)

where ΔQ_k^{ord} is defined as:

$$\Delta Q_k^{\text{ord}} = \sum_i \sum_{i\neq j} \Delta Q_{kij}^{\text{ord}}\left[y_i^\alpha y_j^\beta - x_i x_j\right]$$ (Eq 30)

and $\Delta Q_{kij}^{\text{ord}}$ are the contributions to the activation energy for component k as a result of the chemical ordering of the i and j atoms on the two sublattices; x_i is the mole fraction of component i; and y_i^α and y_i^β are the site fractions of component i on the given sublattices:

$$y_i^\alpha = \frac{N_i^\alpha}{N_{\text{total}}^\alpha}$$ (Eq 31)

where N_i^α equals the number of i atoms on the α sublattice, and N_{total}^α equals the total number of atoms on the α sublattice. This approach was developed for an AB (B2) alloy where diffusion occurs via jumps between two metal sublattices; however, the approach is also valid for A_3B (Fe_3Al) alloys (DO_3 ordering) (Ref 45), where diffusion occurs via a network of nearest-neighbor jumps and where the fcc or hexagonal close-packed crystal structure is the base for the ordered phase. This model has been successfully used to describe the Fe-Ni-Al diffusion in the B2 phase (Ref 34) and to describe the Ni-Al-Cr diffusion in the B2 and γ' phases (Ref 46).

Stoichiometric Phases

For binary stoichiometric phases, the diffusivity is assumed to be proportional to the difference in the chemical potentials at each end of the stoichiometric phase multiplied by the mobility for the component in the phase. Tracer diffusivity data for the component in the stoichiometric phase are used to assess the diffusion mobility functions. This type of model has been applied to the diffusivity of carbon in cementite (Ref 47).

Determination of Diffusion Mobility Coefficients

Similar to the Gibbs energy function coefficients used in multicomponent thermodynamic databases, the diffusion mobility parameters in Eq 26 and 30 are determined from experimental data for each system and can be evaluated using trial-and-error methods or mathematical methods that minimize the error between the calculated and experimental diffusion coefficients, as indicated in Fig. 8. The trial-and-error method is only feasible if a few different data types are available. This method becomes increasingly cumbersome as the number of components and/or number of data types increases. When this occurs, mathematical methods, such as the least-squares method of Gauss (Ref 48), the Marquardt method (Ref 49), or the Bayesian estimation method (Ref 50), are more efficient. The PARROT optimizer (Ref 51) within the DICTRA code (Ref 52, 53) allows direct optimization of diffusion mobility functions.

General Principles. The same principles guiding the assessment of thermodynamic data (Ref 28) also apply to diffusion data, with a few additional constraints. First, a thermodynamic database (or description) must be selected to calculate the needed thermodynamic factors for intrinsic and interdiffusion coefficients. In choosing a thermodynamic database,

the phase models used for the thermodynamics must be the same as those used in the diffusion mobility database. For example, if a thermodynamic description uses a two-sublattice model of an fcc phase (one sublattice for the substitutional elements and a second sublattice for the interstitials), then the same two-sublattice model must be used in the diffusion mobility database. After selecting a thermodynamic database/description to use for developing the diffusion mobility database, a critical evaluation of all the available data must be performed. As the tracer diffusivity data are not dependent on the thermodynamics, these data are preferred and often weighted more heavily than other diffusivity data, which are dependent on the thermodynamic description used. The assessment process continues by optimizing the mobility parameters for each component in each phase separately and then optimizing the mobility parameters for all of the components in a given phase with all of the relevant, and appropriately weighted, diffusion data. Zero-order binary and ternary interaction parameters may be added as needed to fit the available diffusion data. Generally, ternary and higher-order binary interactions are rarely needed to fit the experimental data, or there are insufficient experimental data to justify such terms. After all of the needed mobility parameters are optimized, the assessment is verified using diffusion data not considered during optimization, such as a comparison of calculated and measured composition profiles from diffusion-couple experiments. The assessed parameters may also be evaluated by comparing activation energies with diffusion correlations published in the literature (Ref 54) or with first-principles calculations.

Binary Assessment Example. The assessment of the nickel-tungsten diffusion mobilities in the fcc phase is described here as an example. The thermodynamic description developed by Gustafson et al. (Ref 55) is used. The fcc phase is modeled using a two-sublattice description (nickel, tungsten: vacancies), where nickel and tungsten occupy the substitutional sublattice, and vacancies occupy the interstitial sublattice. For the nickel-tungsten system in the fcc phase, both tracer (Ref 56) (Fig. 9) and interdiffusion (Ref 57) (Fig. 10) data are available. The nickel and tungsten diffusion mobilities in the fcc phase are described as:

$$M_i = \frac{1}{RT}\exp\left(\frac{\Delta Q_i'}{RT}\right) \text{ where } i = \text{Ni, W}$$ (Eq 32)

$$\Delta Q_{\text{Ni}}' = x_{\text{Ni}}Q_{\text{Ni}}^{\text{Ni}} + x_{\text{W}}Q_{\text{Ni}}^{\text{W}} + x_{\text{Ni}}x_{\text{W}}\,^0A_{\text{Ni}}^{\text{Ni,W}}$$
$$\Delta Q_{\text{W}}' = x_{\text{Ni}}Q_{\text{W}}^{\text{Ni}} + x_{\text{W}}Q_{\text{W}}^{\text{W}} + x_{\text{Ni}}x_{\text{W}}\,^0A_{\text{W}}^{\text{Ni,W}}$$
(Eq 33)

(Note that because this phase has no ferromagnetic contribution, the mobilities are expressed using Eq 28.) If a ferromagnetic contribution were present, separate composition-dependent functions for the activation energy and preexponential terms would be needed (Eq 26).
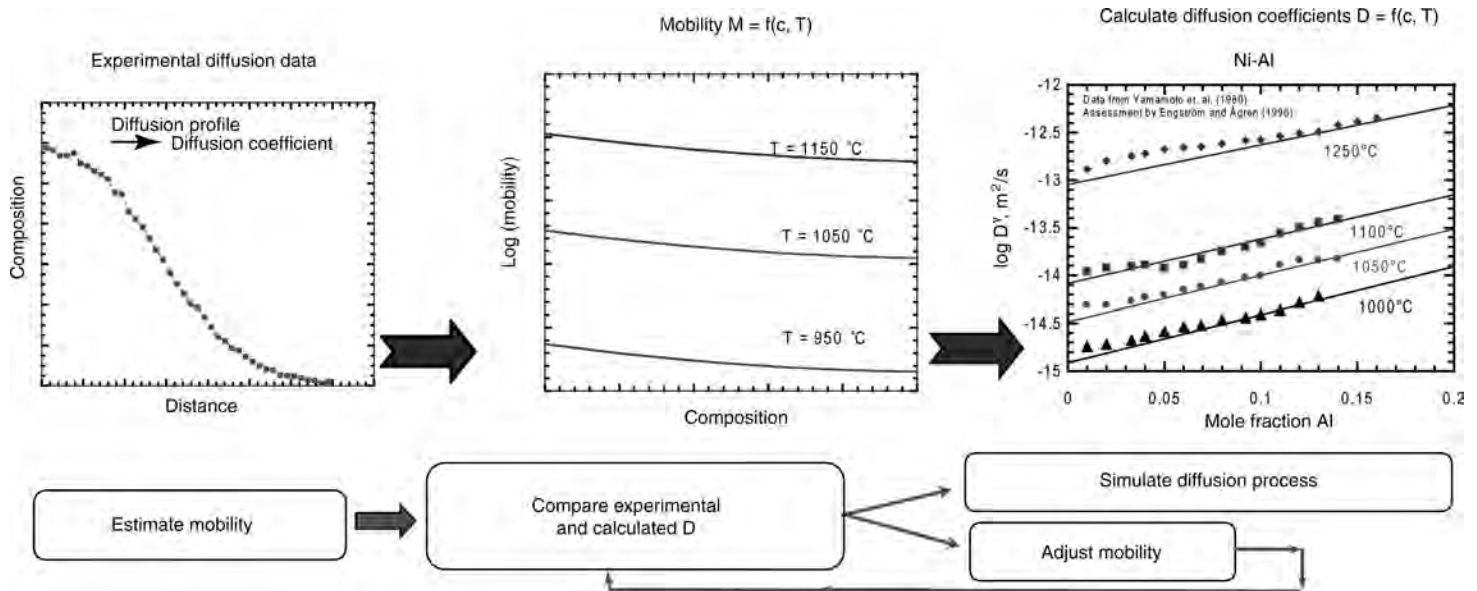
Experimental diffusion data

Mobility M = f(c, T)

Calculate diffusion coefficients D = f(c, T)

Fig. 8 Schematic of diffusion mobility parameter optimization procedure

Q_{Ni}^{Ni} is the self-activation energy for diffusion of nickel in pure fcc nickel; it is well established experimentally, and the mobility parameters are previously determined in the assessment work by Ref 32. Two metastable end-member self-activation energies must be determined: one for the diffusion of tungsten in pure fcc tungsten, Q_W^W, and one for nickel in pure fcc tungsten, Q_{Ni}^W. Because these quantities cannot be measured experimentally (fcc tungsten is not stable), they are determined during the optimization, using diffusion correlations or first principles as initial estimates. The activation energy for tungsten diffusing in fcc nickel, Q_W^{Ni}, is determined using the available tracer and interdiffusion data. The three activation energies are modeled using the following form, where B and C are constants:

$$B + RT \ln(C) \tag{Eq 34}$$

The binary interaction parameters, $^0A_{Ni}^{Ni,W}$ and $^0A_W^{Ni,W}$, are also considered in the optimization and are modeled using a constant value.

To start the assessment, the initial values for the activation energies are all set to equal the value of nickel in pure nickel: $-28{,}700 + 69.8*T$ (Ref 32) (Table 3). The binary interaction parameters are initially set to zero. Note that with this initial set of parameters, there is no concentration dependence for the tracer diffusivities. As seen in Fig. 9(a, b), the tracer diffusivities for all three alloy compositions are equal, using the initial parameters. The first parameters optimized are activation energies for the diffusion of tungsten in pure tungsten and nickel, Q_W^W and Q_W^{Ni}, using the tungsten tracer diffusivity data from Ref 56. The optimization is done by comparing the diffusivities calculated using the values defined for Eq 33 in Eq 13 and the experimental values:

$$D_W^*(x_W, T) =$$

$$\frac{1}{RT} \exp\left(\frac{\left(x_{Ni}Q_W^{Ni} + x_W Q_W^W + x_{Ni}x_W\,^0A_W^{Ni,W}\right)}{RT}\right) \tag{Eq 35}$$

After these parameters are optimized, the binary interaction term, $^0A_W^{Ni,W}$, is optimized, using a start value of -5000 J/mol. Once the tungsten mobility parameters have been optimized using tracer diffusivity data, the values for Q_W^{Ni}, Q_W^W, and $^0A_W^{Ni,W}$ are then fixed, and the nickel mobility parameters (Q_{Ni}^W and $^0A_{Ni}^{Ni,W}$) are optimized using the nickel tracer diffusivity data. After these nickel mobility values are optimized, all of the mobility values (excluding the values for Q_{Ni}^{Ni}) are optimized using both the tracer diffusivity data and the interdiffusion data. Again, the optimized parameters are used to calculate the tracer and interdiffusion diffusivities given by Eq 13 and 15 and then compared to the experimental data. The optimized mobility parameters are listed in Table 3.

The comparison of the diffusivities calculated with the optimized parameters and the experimental values are shown in Fig. 9 and 10. Good agreement between the measured and calculated tracer diffusivity and interdiffusion coefficients is achieved. Other recent diffusion mobility assessment examples are given in the literature by Ref 58 to 60.

In addition to optimizing the mobility functions using various composition-dependent diffusion coefficient data, diffusion mobility functions can be optimized directly from experimental composition profiles. Both Ref 61 and 62 developed methods that combine DICTRA with an optimization tool (MatLab or Mathematica) to assess the mobility parameters from

experimental composition profiles. For a given set of mobility parameters, the difference between the experimental composition and calculated composition is defined by a least-squares error function. The mobility parameters are optimized to minimize the error. This method has been successfully demonstrated for binary and ternary systems.

Strengths and Weaknesses of Assessment Method. The Calphad-based approach to modeling the diffusion mobilities provides an efficient representation of the composition dependence in multicomponent systems. The reduced number of parameters needed to describe diffusion in a multicomponent system occurs as a result of the assumption that the correlation factors are negligible in the lattice-fixed frame of reference, and only the diagonal terms of the mobility matrix must be evaluated. However, if the vacancy concentration is not in local equilibrium, the off-diagonal terms resulting from the correlation factors should be considered (Ref 5, 19). Using the Calphad method to describe the composition dependence of the mobility terms requires the determination of mobilities for fictive metastable end-member phases. Examples of such quantities are the mobility of tungsten in fcc tungsten and the mobility of tungsten in fcc aluminum at temperatures above the fcc aluminum melting temperature (e.g., 1300 °C). Determination of these end-member quantities may follow approaches similar to those used to determine the lattice stabilities of the metastable thermodynamic quantities of the elements (Ref 26–28). This determination of diffusion-activation energies for fictive end-member phases may appear to limit the Calphad method; however, it is these determinations that enable the extrapolation to higher-order systems where diffusion data are limited.

These optimization methods have been employed to develop several commercial
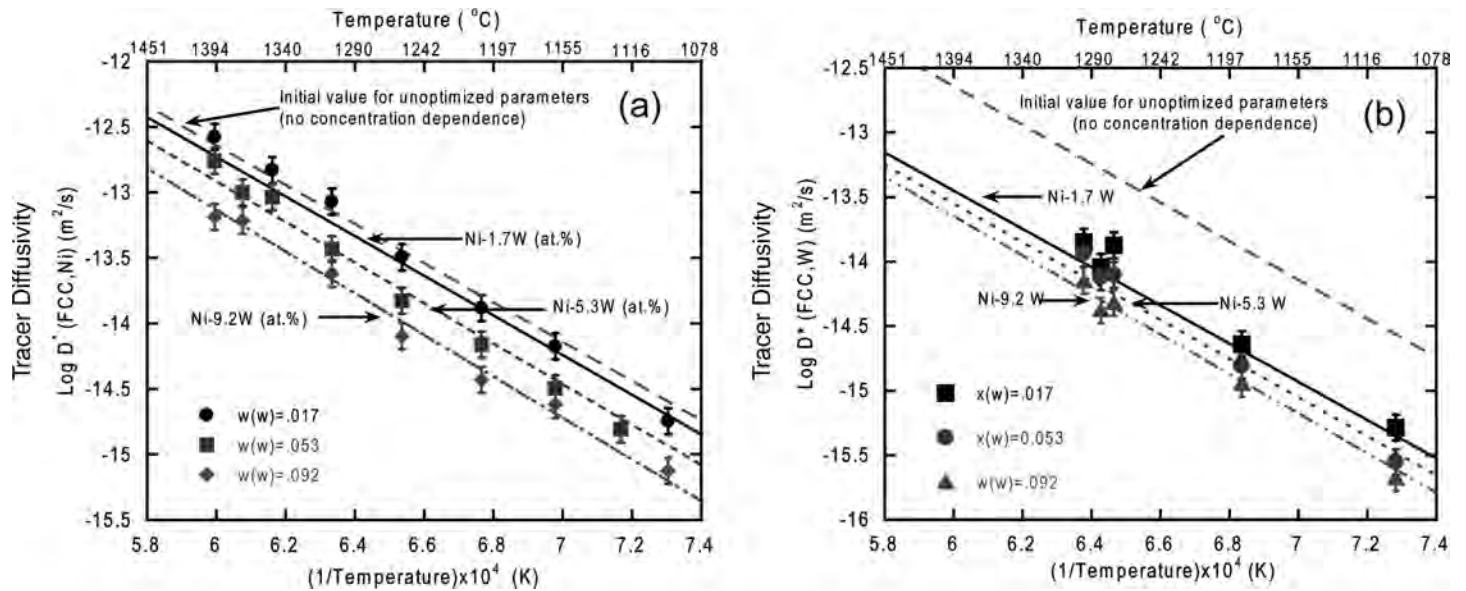
Fig. 9 Comparison of calculated and measured tracer diffusivity data for (a) nickel and (b) tungsten in nickel-tungsten face-centered cubic (fcc) alloys as functions of temperature. The diffusivities are calculated before and after optimizing the nickel-tungsten system. Note: Before the system optimizes, there is no composition dependence in the mobility functions. Experimental data from Ref 56
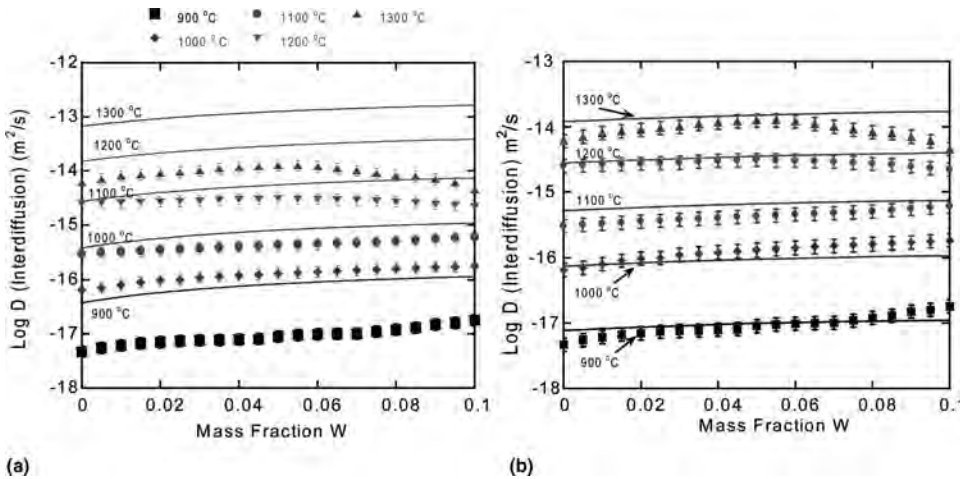

Fig. 10 Comparison of calculated and measured interdiffusion coefficients for the nickel-tungsten system as a function of composition for temperatures ranging from 900 to 1300 °C. (a) Calculated diffusivities before optimization; observed composition dependence is entirely from the composition dependence of the chemical potentials. (b) Calculated diffusivities after the nickel-tungsten system has been optimized. Source: Ref 57

Table 3 Optimized mobility parameters for the nickel-tungsten system

Parameter	Initial values, J/mol	Optimized value, J/mol
Q_{Ni}^{Ni}	$-28{,}700 - 69.8*T$ (Ref 32)	$-28{,}700 - 69.8*T$ (not optimized)
Q_{Ni}^{W}	$-287{,}000 - 69.8*T$	$-628{,}250 + RT$ $\ln(4.78 \times 10^{-4})$
Q_{W}^{W}	$-287{,}000 - 69.8*T$	$-411{,}423 + RT$ $\ln(2.18 \times 10^{-4})$
Q_{W}^{Ni}	$-287{,}000 - 69.8*T$	$-282{,}130 + RT$ $\ln(2.80 \times 10^{-5})$
$^{0}A_{Ni}^{Ni,W}$	$+ 0.0$	$+175{,}736$
$^{0}A_{W}^{Ni,W}$	$+ 0.0$	$-97{,}025$

Table 4 Available mobility databases

Database name/alloy system	Reference
MOB2 (general-purpose database, with emphasis on iron-base alloys	Ref 63
MOBAl1 (aluminum-base alloys)	Ref 63
MOBNi1	Ref 63
NIST-NiMob (face-centered cubic nickel-base alloys)	Ref 64
Cobalt-base alloys (face-centered cubic phase)	Ref 65
Solder alloys	Ref 66, 67
Zirconium-base alloys	Ref 68
Cemented carbides	Ref 69, 70

diffusion mobility databases, as well as many smaller databases for specific research applications. Table 4 lists several of the commercial and research databases available. All of these databases can be employed by a variety of diffusion codes, finite-difference codes that assume local equilibrium at each grid point (e.g., DIC-TRA), random walk methods (Ref 71), and phase-field codes.

Application

Single-Phase Diffusion. The most common diffusion simulation is the diffusion of one single-phase material into another at constant temperature and pressure. The results of these simulations are generally shown as composition profiles as a function of distance at a specified time. The complexity associated with an 11-component nickel-base superalloy diffusion couple is demonstrated in Fig. 11, where the interdiffusion between two single-phase γ(fcc) nickel-base superalloys (René-N4/René-N5) after 100 h at 1293 °C (Ref 72) is shown. The predictions were made using the DICTRA software in conjunction with the National Institute of Standards and Technology (NIST)-NiMob diffusion mobility database (Ref 64) and the Thermotech Ni-Data thermodynamic database (Ref 73). In addition to accurately predicting the composition profiles, the diffusion simulation also predicts the location of the maximum pore formation resulting from Kirkendall porosity. Figure 12(a) shows the predicted location of the maximum pore formation, given by the maximum of the negative derivative of the vacancy flux with respect to distance (Ref 74), and Fig. 12(b) reveals that the predicted location corresponds well to the location of Kirkendall porosity observed on the René-N4 side of the diffusion couple.
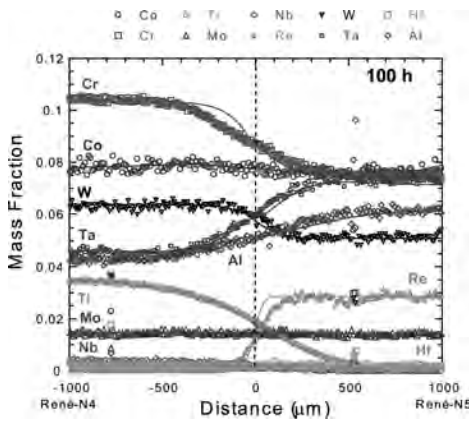
Fig. 11 Calculated (solid lines) and experimental (symbols) composition profiles for René-N4/René-N5 diffusion couples after 100 h at 1293 °C. Source: Ref 72
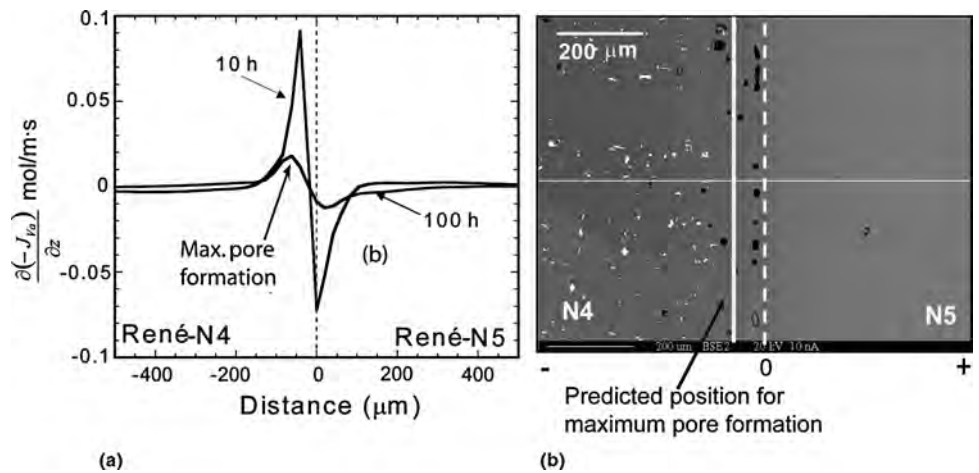

(a)

(b)

Fig. 12 (a) Predicted location of the maximum pore density for a René-N4/René-N5 diffusion couple at 1293 °C. (b) Backscattered image of René-N4/René-N5 diffusion couple after 100 h at 1293 °C. The thin white line indicates the position of the microprobe scan. The dashed white line corresponds to the Matano interface. The dashed line is the location of the predicted maximum porosity. Source: Ref 72
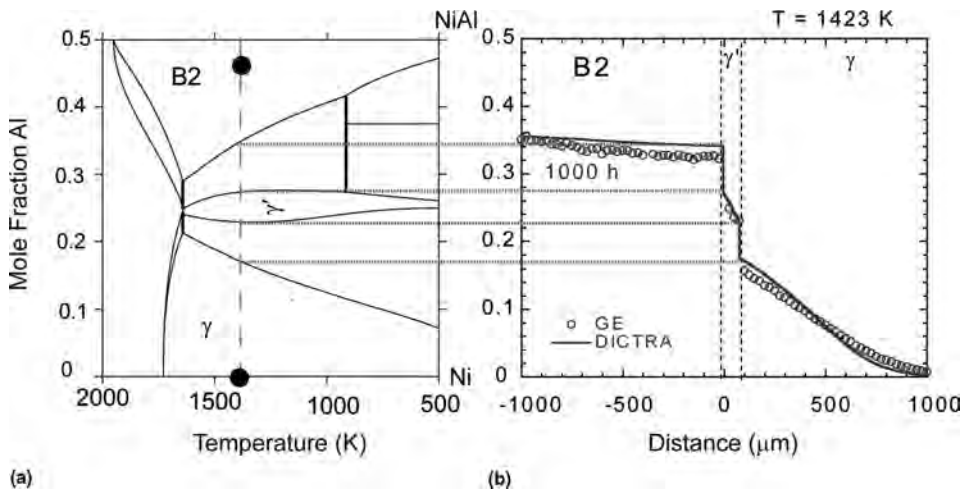

(a)

(b)

Fig. 13 Example of multiphase diffusion in the nickel-aluminum system at 1423 K. (a) The Ni-NiAl section of the nickel-aluminum phase diagram, where the solid circles indicate the initial end-member compositions of the diffusion couple. (b) The measured (open symbols) and calculated (solid line) composition profiles for the Ni-NiAl diffusion couple at 1423 K. Vertical dashed lines indicate the position of the Ni₃Al (γγ') region. The horizontal dashed lines extending between (a) and (b) demonstrate that the positions of the measured and calculated composition jumps corresponding to the different phase regions on the phase diagram. Source: Ref 46

Multiphase Diffusion. The formation of an additional phase is also a common occurrence during the diffusion process between two single-phase materials. Figure 13 shows the formation of a Ni₃Al (gamma prime, γ') layer between the NiAl-B2 and fcc nickel diffusion couple after heat treating for 1000 h at 1150 °C (1423 K). The Ni-NiAl section of the nickel-aluminum phase diagram is shown in Fig. 13(a). In Fig. 13(b), both the measured and predicted composition profiles show the formation of a Ni₃Al (gamma prime) layer between the initially present NiAl-B2 and nickel layers. The dashed lines between Fig. 13(a) and (b) show how the jumps in the composition profiles relate to the phase boundaries on the phase diagram.

In addition to the complexity of multicomponent single-phase diffusion couples, industrially relevant diffusion simulations often involve complicated time-temperature schedules and the precipitation and dissolution of a variety of different phases, both as planar layers and dispersed particles. These simulations are characterized by a variety of outputs, including the position of a moving phase boundary as a function of time, phase fraction profiles, particle-size diameters during coarsening, and locations of Kirkendall porosity. These outputs are essential in optimizing heat treating cycles and solidification schedules, predicting service lifetimes, and determining weldability. Examples of the complex uses of diffusion data to predict

microstructure evolution are found in other articles of this Handbook.

Appendix 1: Example of Diffusion Matrices for the Ni-0.05Al-0.10Cr fcc Composition at 1200 °C

The following is an example of the calculation of the various diffusion matrices for a ternary Ni-Al-Cr system, for a given set of diffusion mobilities and chemical potentials. The diffusion mobilities and chemical potentials are calculated using the data from Engström (Ref 33) and the SSOL4 substance database (Ref 75), respectively.

For the given Ni-0.05Al-0.1Cr (atomic fraction) composition at 1200 °C, the diffusion mobilities, in a lattice-fixed frame of reference, assuming the correlation effects are negligible, are given as:

$$^L M_{ik} = \delta_{ik}x_iM_i = \begin{bmatrix} & Al & Cr & Ni \\ Al & (0.05\cdot4.25) & 0 & 0 \\ Cr & 0 & (0.10\cdot2.35) & 0 \\ Ni & 0 & 0 & (0.85\cdot1.75) \end{bmatrix} \cdot 10^{-18} m^2/s$$

$$= \begin{bmatrix} & Al & Cr & Ni \\ Al & 2.12 & 0 & 0 \\ Cr & 0 & 2.35 & 0 \\ Ni & 0 & 0 & 14.9 \end{bmatrix} \cdot 10^{-19} m^2/s$$

(Eq 1.1)

Assuming nickel is the dependent variable, the matrix of chemical potentials at 1200 °C is given by:

$$\left[\frac{\partial\mu_k}{\partial x_j}\right] = \begin{bmatrix} & Al & Cr & Ni \\ Al & +39.2 & +9.23 & +0 \\ Cr & +8.60 & +18.3 & +0 \\ Ni & -3.32 & -2.70 & +0 \end{bmatrix} \cdot 10^4 (J/mol)$$

(Eq 1.2)

The tracer diffusivities for the Ni-5Al-10Cr composition at 1200 °C are then calculated using Eq 13:

$$\mathbf{D}^* = \begin{bmatrix} \text{Al} & 5.20 \\ \text{Cr} & 2.87 \\ \text{Ni} & 2.14 \end{bmatrix} \cdot \left(\times 10^{-14} \, \text{m}^2/\text{s} \right) \qquad \text{(Eq 1.3)}$$

The diffusion matrix in the lattice frame of reference is the product of the mobility matrix (Eq 1.1) times the chemical potential matrix (Eq 1.2), as defined in Eq 21:

$$\begin{aligned}
{}^{\mathbf{L}}\mathbf{D} &= (\delta_{xi} x_i [\mathbf{M}]) \times \left[\frac{\partial \boldsymbol{\mu}_{\mathbf{k}}}{\partial \mathbf{x_j}} \right] \\
&= \begin{bmatrix} & \text{Al} & \text{Cr} & \text{Ni} \\ \text{Al} & +8.33 & +1.96 & +0 \\ \text{Cr} & +2.09 & +4.30 & +0 \\ \text{Ni} & -4.95 & -4.02 & +0 \end{bmatrix} \cdot 10^{-14} \, (\text{m}^2/\text{s})
\end{aligned}$$

(Eq 1.4)

The diffusion matrix in the volume-fixed frame of reference, assuming constant molar volumes, is given by Eq 15:

$$\begin{aligned}
{}^{\mathbf{V}}\mathbf{D_{kj}^{n}} &= (\delta_{ik} - x_k) x_i \mathbf{M} \times \frac{\partial \mu_i}{\partial \mathbf{x_j}} \\
&= \begin{bmatrix} & \text{Al} & \text{Cr} & \text{Ni} \\ \text{Al} & 2.02 & -0.12 & -0.74 \\ \text{Cr} & -0.21 & 2.11 & -1.49 \\ \text{Ni} & -1.81 & -1.99 & 2.23 \end{bmatrix} \cdot 10^{-19} \\
&= \begin{bmatrix} & \text{Al} & \text{Cr} & \text{Ni} \\ \text{Al} & +39.2 & +9.23 & +0 \\ \text{Cr} & +8.60 & +18.3 & +0 \\ \text{Ni} & -3.32 & -2.70 & +0 \end{bmatrix} \cdot 10^{4} \\
&= \begin{bmatrix} & \text{Al} & \text{Cr} & \text{Ni} \\ \text{Al} & +8.06 & +1.85 & +0 \\ \text{Cr} & +1.48 & +4.07 & +0 \\ \text{Ni} & -9.54 & -5.92 & +0 \end{bmatrix} \cdot 10^{-14} \, (\text{m}^2/\text{s})
\end{aligned}$$

(Eq 1.5)

The reduced diffusion matrix in the volume-fixed frame of reference (Eq 15), which is commonly referred to as the interdiffusion coefficient matrix, is defined as the following, where nickel is the dependent variable:

$$\begin{aligned}
{}^{\mathbf{V}}\mathbf{D_{kj}^{Ni}} &= {}^{\mathbf{V}}\mathbf{D_{kj}} - {}^{\mathbf{V}}\mathbf{D_{kn}} \\
{}^{\mathbf{V}}\tilde{D}_{kj}^{Ni} &= \begin{bmatrix} & \text{Al} & \text{Cr} \\ \text{Al} & {}^{\mathbf{V}}D_{AlAl}^{Ni} & {}^{\mathbf{V}}D_{AlNi}^{Ni} \\ \text{Cr} & {}^{\mathbf{V}}D_{CrAl}^{Ni} & {}^{\mathbf{V}}D_{CrCr}^{Ni} \end{bmatrix} \\
{}^{\mathbf{V}}\tilde{D}_{kj}^{Ni} &= \begin{bmatrix} & \text{Al} & \text{Cr} \\ \text{Al} & {}^{\mathbf{V}}D_{AlAl} - {}^{\mathbf{V}}D_{AlNi} & {}^{\mathbf{V}}D_{AlCr} - {}^{\mathbf{V}}D_{AlNi} \\ \text{Cr} & {}^{\mathbf{V}}D_{CrAl} - {}^{\mathbf{V}}D_{CrNi} & {}^{\mathbf{V}}D_{CrCr} - {}^{\mathbf{V}}D_{CrNi} \end{bmatrix} \\
&= \begin{bmatrix} & \text{Al} & \text{Cr} \\ \text{Al} & +8.06 & +1.85 \\ \text{Cr} & 1.48 & +4.07 \end{bmatrix} \cdot 10^{-14} \, (\text{m}^2/\text{s})
\end{aligned}$$

(Eq 1.6)

Using this matrix of interdiffusion coefficients, the flux equations for the specified composition can be written in terms of Eq 16:

$$\tilde{J}_{Al} = -{}^{\mathbf{V}}\tilde{D}_{AlAl}^{Ni} \frac{\partial c_{Al}}{\partial z} - {}^{\mathbf{V}}\tilde{D}_{AlCr}^{Ni} \frac{\partial c_{Cr}}{\partial z} \qquad \text{(Eq 1.7)}$$

$$\tilde{J}_{Cr} = -{}^{\mathbf{V}}\tilde{D}_{CrAl}^{Ni} \frac{\partial c_{Al}}{\partial z} - {}^{\mathbf{V}}\tilde{D}_{CrCr}^{Ni} \frac{\partial c_{Cr}}{\partial z} \qquad \text{(Eq 1.8)}$$

Solution of these flux equations enables the calculation of composition profiles as a function of time in a single-phase region.

REFERENCES

1. A. Fick, Ueber Diffusion, *Poggendorff's Annalen,* Vol 94, 1855 p 59–86
2. A. Fick, *Philos. Mag. A,* Vol 10, S 4, 1855 p 30–39
3. H.S. Carslaw and J.C. Jaeger, *Conduction of Heat in Solids,* Clarendon Press, Oxford, 1959
4. J. Crank, *The Mathematics of Diffusion,* 2nd ed., Clarendon Press, Oxford, 1975
5. J. Philibert, *Atom Movements: Diffusion and Mass Transport in Solids,* Editions de Physique, Les Ulis, France, 1991
6. P. Shewmon, *Diffusion in Solids,* 2nd ed., TMS, Warrendale, PA, 1989
7. L. Boltzmann, *Ann. Physik,* Vol 53, 1894, p 960
8. C. Matano, *Jpn. J. Phys.,* Vol 8, 1933, p 109
9. A. Paul, A.A. Kodentsov, and F.J.J. van Loo, On Diffusion in the β-NiAl Phase, *J. Alloy. Compd.,* Vol 403, 2005, p 147–153
10. V.F. Sauer and V. Freise, Diffusion in binren Gemischen mit Volumennderung, *Z. Elektrochem.,* Vol 66 (No. 4), 1962, p 353–363
11. F.J.A. d. Broeder, A General Simplification and Improvement of the Matano-Boltzmann Method in the Determination of the Interdiffusion Coefficients in Binary Systems, *Scr. Metall.,* Vol 3, 1969, p 321–326
12. C. Wagner, The Evaluation of Data Obtained with Diffusion Couples of Binary Single-Phase and Multiphase System, *Acta Metall.,* Vol 17 (No. 2), 1969, p 99–107
13. M.A. Dayananda, Average Effective Interdiffusion Coefficients and the Matano Plane Composition, *Metall. Mater. Trans. A,* Vol 27 (No. 9), 1996, p 2504–2509
14. M.A. Dayananda, MultiDiFlux, Purdue University, West Lafayette, IN, 2005, https://engineering.purdue.edu/MSE/Research/MultiDiFlux/index.htm
15. E.O. Kirkendall, Diffusion of Zinc in Alpha Brass, *Trans. AIMME,* Vol 147, 1942, p 104–110
16. A.D. Smigelskas and E.O. Kirkendall, Zinc Diffusion in Alpha-Brass, *Trans. AIMME,* Vol 171, 1947, p 130–142
17. L.S. Darken, Diffusion, Mobility and Their Interrelation through Free Energy in Binary Metallic Systems, *Trans. AIMME,* Vol 175, 1948, p 184–201
18. J.R. Manning, Diffusion and the Kirkendall Shift in Binary Alloys, *Acta Metall.,* Vol 15 (No. 5), 1967, p 817–826
19. J.R. Manning, Cross Terms in the Thermodynamic Diffusion Equations for Multicomponent Alloys, *Metall. Trans.,* Vol 1 (No. 2), 1970, p 499–505
20. A. Janotti, M. Krcmar, C.L. Fu, and R.C. Reed, Solute Diffusion in Metals: Larger Atoms Can Move Faster, *Phys. Rev. Lett.,* Vol 92 (No. 8), 2004, p 085901-1
21. Y. Mishin and D. Farkas, Atomistic Simulation of Point Defects and Diffusion in B2 NiAl: Part I: Point Defect Energetics, *Philos. Mag. A,* Vol 75 (No. 1), 1997, p 169–185
22. Y. Mishin and D. Farkas, Atomistic Simulation of Point Defects and Diffusion in B2 NiAl: Part II: Diffusion Mechanisms, *Philos. Mag. A,* Vol 75 (No. 1), 1997, p 187–199
23. Y. Mishin, A. Lozovoi, and A. Alavi, Evaluation of Diffusion Mechanisms in NiAl by Embedded-Atom and First-Principles Calculations, *Phys. Rev. B,* Vol 67, 2003, p 014201
24. A. Van der Ven, G. Ceder, M. Asta, and P.D. Tepesch, First-Principles Theory of Ionic Diffusion with Nondilute Carriers, *Phys. Rev. B,* Vol 64, 2001, p 184307
25. H.-C. Yu, D.-H. Yeon, A. Van der Ven, and K. Thornton, Substitutional Diffusion and Kirkendall Effect in Binary Crystalline Solids Containing Discrete Sources and Sinks, *Acta Mater.,* Vol 55, 2007, p 6690–6704
26. L. Kaufman and H. Bernstein, *Computer Calculation of Phase Diagrams,* Academic Press, London, 1970
27. N. Saunders and A.P. Miodownik, *CALPHAD Calculation of Phase Diagrams: A Comprehensive Guide,* R.W. Cahn, Ed., Elsevier Science Inc., New York, 1998
28. H. Lukas, S.G. Fries, and B. Sundman, *Computational Thermodynamics: The CALPHAD Method,* Cambridge University Press, Cambridge, 2007
29. J.-O. Andersson and J. Ågren, Models for Numerical Treatment of Multicomponent Diffusion in Simple Phases, *J. Appl. Phys.,* Vol 72 (No. 4), 1992, p 1350–1355
30. O. Redlich and A. Kister, Algebraic Representation of Thermodynamic Properties and the Classification of Solutions, *Ind. Eng. Chem.,* Vol 40 (No. 2), 1948, p 345–348
31. B. Jönsson, Assessment of the Mobilities of Cr, Fe and Ni in bcc Cr-Fe-Ni Alloys, *ISIJ Int.,* Vol 35 (No. 11), 1995, p 1415–1421
32. B. Jönsson, Assessment of the Mobilities of Cr, Fe, and Ni in fcc Cr-Fe-Ni Alloys, *Z. Metallkd.,* Vol 86 (No. 10), 1995, p 686–692
33. A. Engström and J. Ågren, Assessment of Diffusional Mobilities in Face-Centered Cubic Ni-Cr-Al Alloys, *Z. Metallkd.,* Vol 87 (No. 2), 1996, p 92–97
34. T. Helander and J. Ågren, Diffusion in the B2-BCC Phase of the Al-Fe-Ni System—Application of a Phenomenological Model, *Acta Mater.,* Vol 47 (No. 11), 1999, p 3291–3300
35. T. Helander and J. Ågren, A Phenomenological Treatment of Diffusion in Al-Fe and Al-Ni Alloys Having B2-BCC Ordered Structure, *Acta Mater.,* Vol 47 (No. 4), 1999, p 1141–1152
36. J. Kucera and B. Million, *Metall. Trans. A,* Vol 1, 1970 p 2603–2606
37. J. Ågren, Diffusion in Phases with Several Components and Sublattices, *J. Phys. Chem. Solids,* Vol 43 (No. 5), 1982, p 421–430

38. B. Jönsson, Assessment of the Mobility of Carbon in fcc C-Cr-Fe-Ni Alloys, *Z. Metallkd.*, Vol 85 (No. 7), 1994, p 502–509

39. B. Jönsson, On Ferromagnetic Ordering and Lattice Diffusion—A Simple Model, *Z. Metallkd.*, Vol 83 (No. 5), 1992, p 349–355

40. B. Jönsson, Ferromagnetic Ordering and Diffusion of Carbon and Nitrogen in Bcc Cr-Fe-Ni Alloys, *Z. Metallkd.*, Vol 85 (No. 7), 1994, p 498–501

41. R. Braun and M. Fellerkniepmeier, On the Magnetic-Anomalies of Self-Diffusion and Heterodiffusion in Bcc-Iron, *Scr. Metall.*, Vol 20 (No. 1), 1986, p 7–11

42. J. Ågren, Computer Simulation of the Austenite/Ferrite Diffusional Transformation in Low Alloyed Steels, *Acta Metall.*, Vol 30, 1982, p 841–851

43. J. Ågren, Complex Simulations of Diffusional Reactions in Complex Steels, *ISIJ Int.*, Vol 32 (No. 3), 1992, p 291–296

44. L.A. Girifalco, Vacancy Concentration and Diffusion in Order-Disorder Alloys, *J. Phys. Chem. Solids*, Vol 24, 1964, p 323–333

45. Z. Tôkei, J. Bernardini, P. Gas, and D.L. Beke, Volume Diffusion of Iron in Fe₃Al: Influence of Ordering, *Acta Mater.*, Vol 45 (No. 2), 1997, p 541–546

46. C.E. Campbell, Assessment of the Diffusion Mobilities in the Ni-Al-Cr B2 and γ′ phases, *Acta Mater.*, Vol 56 (No. 16), 2008, p 4277–4290

47. M. Hillert, L. Hoglund, and J. Agren, Diffusion in Interstitial Compounds with Thermal and Stoichiometric Defects, *J. Appl. Phys.*, Vol 98 (No. 5), 2005, p 053511

48. H.L. Lukas, E.T. Henig, and B. Zimmermann, Optimization of Phase-Diagrams by a Least-Squares Method Using Simultaneously Different Types of Data, *Calphad*, Vol 1 (No. 3), 1977, p 225–236

49. D.W. Marquardt, An Algorithm for Least-Squares Estimation of Nonlinear Parameters, *J. Soc. Ind. Appl. Math.*, Vol 11 (No. 2), 1963, p 431–441

50. E. Konigsberger, Improvement of Excess Parameters from Thermodynamic and Phase-Diagram Data by a Sequential Bayes Algorithm, *Calphad*, Vol 15 (No. 1), 1991, p 69–78

51. B. Jansson, "PARRssOT, " Report TRITA-MAC-0234, Royal Institute of Technology, Stockholm Sweden,1984

52. J.O. Andersson, T. Helander, L. Höglund, P.F. Shi, and B. Sundman, Thermo-Calc and DICTRA, Computational Tools for Materials Science, *Calphad*, Vol 26, 2002, p 273–312

53. A. Borgenstam, A. Engström, L. Höglund, and J. Ågren, DICTRA, A Tool for Simulation of Diffusion Transformations in Alloys, *J. Phase Equil.*, Vol 21 (No. 3), 2000, p 269–280

54. A.M. Brown and M.F. Ashby, Correlations for Diffusion Constants, *Acta Metall.*, Vol 28, 1980, p 1085–1101

55. P. Gustafson, A. Gabriel, and I. Ansara, A Thermodynamic Evaluation of the C-Ni-W System, *Z. Metallkd.*, Vol 28, 1987, p 151–156

56. K. Monma, H. Suto, and H. Oikawa, Diffusion of Ni-63 and W-185 in Ni-W Alloys, *J. Jpn. Inst. Met.*, Vol 28, 1964, p 197–200

57. M.S.A. Karunaratne, P. Carter, and R.C. Reed, Interdiffusion in the fcc-Centred Cubic Phase of the Ni-Re, Ni-Ta, and Ni-W Systems between 900 and 1300 °C, *Mater. Sci. Eng. A*, Vol 281, 2000, p 229–233

58. Y.W. Cui, K. Oikawa, R. Kainuma, and K. Ishida, Study of Diffusion Mobility of Al-Zn Solid Solution, *J. Phase Equil. Dif.*, Vol 27 (No. 4), 2006, p 333–342

59. L. Zhang, Y. Du, Y. Ouyang, H. Xu, X.-G. Lu, Y. Liu, Y. Kong, and J. Wang, Atomic Mobilities, Diffusivities and Simulation of Diffusion Growth in the Co-Si System, *Acta Mater.*, Vol 56, 2008, p 3940–3950

60. J. Wang, L.B. Liu, H.S. Liu, and Z.P. Jin, Assessment of the Diffusional Mobilities in the Face-Centred Cubic Au-Ni Alloys, *Calphad*, Vol 31 (No. 2), 2007, p 249–255

61. C.E. Campbell, A New Technique for Evaluating Diffusion Mobility Parameters, *J. Phase Equil. Dif.*, Vol 26 (No. 5), 2005, p 435–440

62. L. Höglund, DICTRA ToolBox, Thermo-Calc AB, Stockholm, Sweden, 2004

63. Thermo-Calc Software, http://www.thermocalc.com/

64. C.E. Campbell, W.J. Boettinger, and U.R. Kattner, Development of a Diffusion Mobility Database for Ni-Base Superalloys, *Acta Mater.*, Vol 50, 2002, p 775–792

65. T. G¢mez-Acedbo, B. Navarcorena, and F. Castro, Interdiffusion in Multiphase, Al-Co-Cr-Ni-Ti Diffusion Couples, *J. Phase Equil. Dif.*, Vol 25 (No. 3), 2004, p 237–251

66. G. Ghosh, Dissolution and Interfacial Reactions of Thin-Film Ti/Ni/Ag Metallizations in Solder Joints, *Acta Mater.*, Vol 49 (No. 14), 2001, p 2609–2624

67. G. Ghosh and Z.K. Liu, Modeling the Atomic Transport Kinetics in High-Lead Solders, *J. Electron. Mater.*, Vol 27 (No. 12), 1998, p 1362–1366

68. C. Toffolon-Masclet, M. Mathon, A. Engström, and J.C. Brachet, in *14th International Symposium on Zirconium in the Nuclear Industry* (Stockholm, Sweden), 2004

69. Y.L. He, L. Li, S.G. Huang, J. Vleugels, and O. Van der Bies, Computer Simulation of W-C-Co-V System Diffusion Couples, *Rare Met.*, Vol 26 (No. 5), 2007, p 492–497

70. S. Haglund and J. Ågren, *Acta Mater.*, Vol 46 (No. 8), 1998, p 2801–2807

71. H. Larsson and J. Ågren, Combined Probability Distributions of Random-Walks: A New Method to Simulate Diffusion Processes, *Comput. Mater. Sci.*, Vol 34, 2005, p 254–263

72. C.E. Campbell, W.J. Boettinger, T. Hansen, P. Merewether, and B.A. Mueller, Examination of Multicomponent Diffusion Between Two Ni-Base Superalloys, *Third International Alloy Conference* (Lisbon, Portugal), Springer, 2002, p 241–250

73. N. Saunders, Phase Diagram Calculations for Ni-Based Superalloys, *Superalloys 1996* (Warrendale, PA),TMS, 1996, p 101–110

74. L. Höglund and J. Ågren, Analysis of the Kirkendall Effect, Marker Migration and Pore Formation, *Acta Mater.*, Vol 49, 2001, p 1311–1317

75. Scientific Group Thermodata Europe (SGTE), http://www.sgte.org

SELECTED REFERENCES

Diffusion texts

• M.E. Glicksman, *Diffusion in Solids: Field Theory, Solid-State Principles, and Applications*, Wiley-Interscience, 1999

• D. Gupta, *Diffusion Processes in Advanced Technological Materials*, Series William Andrew, Inc., Norwich, New York, 2005

• P. Heitjans and J. Kärger, *Diffusion in Condensed Matter*, Springer, New York, 2005

• J.S. Kirkaldy and D. Young, *Diffusion in the Condensed State*, Institute of Metals, London, 1987

• F.J.J. v. Loo, Multiphase Diffusion in Binary and Ternary Solid-State Systems, *Prog. Solid State Chem.*, Vol 20, 1990, p 47–99

• H. Mehrer, *Diffusion in Solids: Fundamentals, Methods, Materials, Diffusion-Controlled Processes*, Springer, 2007

• J. Philibert, *Atom Movements: Diffusion and Mass Transport in Solids*, Series Editions de Physique, Les Ulis, France, 1991

• P. Shewmon, *Diffusion in Solids*, 2nd ed., TMS, Warrendale, PA, 1989

Critical diffusion data collections

• H. Bakker, H.P. Bonzel, C.M. Bruff, M.A. Dayananda, W. Gust, J. Horvath, I. Kaur, G.V. Kidson, A.D. LeClaire, H. Mehrer, G.E. Murch, G. Neumann, N. Stolica, and N.A. Stolwijk, Ed., *Landolt-Börnstein: Diffusion in Solid Metals and Alloys*, New Series, Group III, Vol 25 and 26, Springer-Verlag, Berlin, 1990

• Diffusion and Defect Forum, http://www.scientific.net/DDF/

• W.F. Gale and T.C. Totemeier, Ed., *Smithells Metals Reference Book*, Elsevier, 2004

• G. Neumann and C. Tuijn, *Self-Diffusion and Impurity Diffusion in Pure Metals: Handbook of Experimental Data*, Elsevier, New York, 2009

• NIMS Diffusion Data, https://kuzuha.nims.go.jp/diffusion/diffusion/index_en.html

• NIST Diffusion Data Center, http://patapsco.nist.gov/diffusion/